

Green Chemistry

Cutting-edge research for a greener sustainable future

Accepted Manuscript

This article can be cited before page numbers have been issued, to do this please use: X. Hu, M. Fan, Y. Zhu, Q. Zhu, Q. Song and Z. Dong, *Green Chem.*, 2019, DOI: 10.1039/C9GC01910C.



This is an Accepted Manuscript, which has been through the Royal Society of Chemistry peer review process and has been accepted for publication.

Accepted Manuscripts are published online shortly after acceptance, before technical editing, formatting and proof reading. Using this free service, authors can make their results available to the community, in citable form, before we publish the edited article. We will replace this Accepted Manuscript with the edited and formatted Advance Article as soon as it is available.

You can find more information about Accepted Manuscripts in the [Information for Authors](#).

Please note that technical editing may introduce minor changes to the text and/or graphics, which may alter content. The journal's standard [Terms & Conditions](#) and the [Ethical guidelines](#) still apply. In no event shall the Royal Society of Chemistry be held responsible for any errors or omissions in this Accepted Manuscript or any consequences arising from the use of any information it contains.

Biomass-Derived Phosphorus-Doped Carbon Materials as Efficient Metal-Free Catalysts for Selective Aerobic Oxidation of Alcohols

Xiwei Hu, Mengying Fan, Yangyang Zhu, Qian Zhu, Qiang Song and Zhengping Dong*

College of Chemistry and Chemical Engineering, Gansu Provincial Engineering Laboratory for Chemical Catalysis, Laboratory of Special Function Materials and Structure Design of the Ministry of Education, Lanzhou University, Lanzhou 730000, PR China

E-mail address: dongzhp@lzu.edu.cn (Zhengping Dong), Tel: 86 931 8912577.

Abstract

Heteroatom-doped carbon materials (HDCMs) with abundant active functional groups and stable structural characteristics are promising catalysts for eco-friendly metal-free catalysis. In this work, phosphorus-doped carbon materials with highly porous structure and extremely high surface area ($>1600 \text{ m}^2 \text{ g}^{-1}$) were successfully prepared via a convenient and scalable strategy using easily available soluble starch and phosphoric acid, which are expected to have good performance in mass-transfer and thus promote the catalytic process. As expected, the as-prepared PC-700 catalyst showed remarkable catalytic performance in aerobic oxidation of benzyl alcohol with a higher TOF value than that of other previously reported heteroatom-doped carbon catalysts. It also exhibited great tolerance for various substrates, including aromatic, alicyclic, heterocyclic, and aliphatic alcohols. On the basis of the related characterizations and experimental results, it was proved that the P-O-C species and the defects caused by P-O species doping on PC-700 catalyst are the active sites for aerobic oxidation. A unique mechanism was proposed for the catalytic process, which is different from that of N-doped graphene and graphene oxide catalyzed reactions that follow a free radical mechanism. In addition, the recycling test and characterizations of the reused catalyst indicate that the PC-700 has extraordinary performance both in recyclability and stability and retain high reactivity even after eight cycles.

1. Introduction

Selective aerobic oxidation of alcohols as an important approach for synthesizing aldehyde intermediates has been widely used in the chemical industry.¹⁻³ Traditionally, oxidants (e.g., chromates, chlorates, and permanganates) and noble metal-based catalysts (e.g., Au and Ru) are frequently used in homogeneous selective aerobic oxidation of alcohols to achieve an ideal yield.⁴⁻⁸ However, the toxicity and corrosivity of these oxidants and the high-cost of noble metal-based catalysts are not in accordance with the principle of “Eco-friendly and Sustainable Chemistry”.⁹ Furthermore, unsustainability in catalytic processes limit the industrial application of homogeneous catalysts.¹⁰ Therefore, widespread and green oxygen sources and environmentally friendly low-cost heterogeneous catalysts are urgently needed for selective aerobic oxidation reactions.

Carbon-based materials that have a lot of heteroatoms-containing active functional groups are considered to be promising heterogeneous catalysts because of their excellent structural stability, high reactivity and remarkable recyclability.^{11, 12} However, common carbon-based materials, such as graphene, GO, and carbon nanotubes, are frequently used as support materials other than heterogeneous catalysts.¹³⁻¹⁶ This is because of their highly ordered structure and the limited active functional groups in their framework. By contrast, HDCMs are efficient catalysts because of their abundant active functional groups, which results from the doping of heteroatoms.¹⁷ Moreover, new defects caused by the differences in atomic radius and bond length between C atoms and those doped heteroatoms generally concentrate a lot of local charges, which is beneficial for in-situ charge transfer from active defect sites to the substrates and thus promoting the reaction.^{18, 19} In fact, the above-mentioned excellent characteristics of HDCMs have already been thoroughly studied in electrocatalysis. For example, such materials have been studied using the oxygen reduction reaction (ORR). Shao *et al.* reported N-doped carbon nanotube arrays as efficient electrocatalysts for ORR with higher reactivity than traditional Pt/C catalysts; their reported electrocatalyst also exhibited outstanding stability.²⁰ The remarkable ORR activity of B and N co-doped carbon nanotubes, which is closely related to the microstructure of the catalyst, has been proved by Yang *et al.*²¹ Dai *et al.* reported that multiwalled P,N-co-doped CNTs are effective ORR catalysts that exhibited outstanding

catalytic performance, and the improved electrocatalytic activity was attributed to the synergistic effect between P and N atoms.²² However, the HDCMs that have been applied as heterogeneous catalysts for chemical synthesis are relatively scarce, and the related mechanisms are still unclear.^{11, 18} Therefore, using carbon materials doped with different heteroatoms as heterogeneous catalysts has significant value for research.

Recently, P-doped carbon materials have been reported in metal-free catalysis because of their unique physico-chemical properties and outstanding catalytic activity.²³⁻²⁵ The lower electronegativity of P atoms compared to that of C atoms and the high electron-donating ability of P atoms make the P dopants positively charged, which is beneficial for charge transfer.^{26, 27} Moreover, large atomic size of P can cause an abundance of defects in the framework of carbon materials. These defects concentrate a lot of charges, which may be the main active sites.^{28, 29} Therefore, because of these unique characteristics of P atoms, P-doped carbon materials may exhibit high reactivity. Additionally, biomass (e.g., sucrose, cellulose, and glucose) are abundant and renewable resources that are frequently used to prepare carbon-based materials.³⁰⁻³⁴ However, the preparation process often involves tedious preprocessing steps, such as alkaline and/or acid activation, and this makes the preparation process time-consuming and environmentally harmful.^{35, 36} By contrast, a method that uses physical mixing and carbonization is more efficient and convenient, which makes it possible to implement such a method in industrial production.

On the basis of these ideas, this work prepared mass-producible P-doped carbon materials (PC-X, where X refers to the carbonization temperature) using biomass soluble starch and low-cost phosphoric acid in an extremely convenient two-step approach. The prepared PC material was applied in the oxidation of alcohols with oxygen as a renewable oxidant.³⁷ The possible active sites were investigated in depth using a series of characterizations and related control experiments. It was demonstrated that P-O-C species and the formation of defects are closely related to the reactivity of aerobic oxidation of alcohols, and this is quite different from the previously reported conclusions.³⁸ Surprisingly, the kinetic study shows that aerobic oxidation catalyzed by PC-700 catalyst has a very low E_a value of 25.70 $\text{KJ}\cdot\text{mol}^{-1}$, which is lower than that of mono-heteroatom-doped, dual-heteroatom-doped, and even noble metal-based catalysts.³⁹⁻⁴¹ Additionally, a unique mechanism was proposed on the basis of all of the above-

mentioned results, which is different from that of other reported heteroatom-doped catalysts (e.g., N-doped graphene).³⁹ In conclusion, this work is expected to offer a new inspiration for fabricating mass-producible biomass-derived heteroatom-doped materials as efficient metal-free catalysts using an extremely simple way for environmentally friendly catalytic applications.

2. Experimental Section

2.1. Materials

Soluble starch, urea, and phosphoric acid (85 wt.%) were purchased from Xilong Chemical Co., Ltd. (China). Aromatic alcohols and aliphatic alcohols were obtained from Sigma-Aldrich Industrial Corp. All of these other reagents were of analytical grade and were used without further purification.

2.2. Preparation of P-doped Carbon Catalysts

Soluble starch (5 g) and phosphoric acid (5.88 g) were added in 30 mL of deionized water with vigorous stirring for 12 h at ambient temperature. The mixture was then dried at 100 °C for 48 h, and the obtained black granular material was ground to powder to obtain PC. The PC powder was pyrolyzed at 500, 600, 700, and 800 °C under a N₂ atmosphere for 2 h with a heating rate of 5 °C min⁻¹ to obtain the PC-X materials. The obtained materials were then treated with 150 mL of boiling water for 2 h to completely remove the P-containing substances. Finally, the treated P-doped carbon materials were dried at 100 °C overnight to obtain PC-500, PC-600, PC-700, and PC-800. The pure carbon catalyst, C-700, was prepared using only soluble starch and pyrolyzed at 700 °C under the same conditions as PC-700.

2.3. Preparation of N-Doped and N,P co-Doped Catalysts

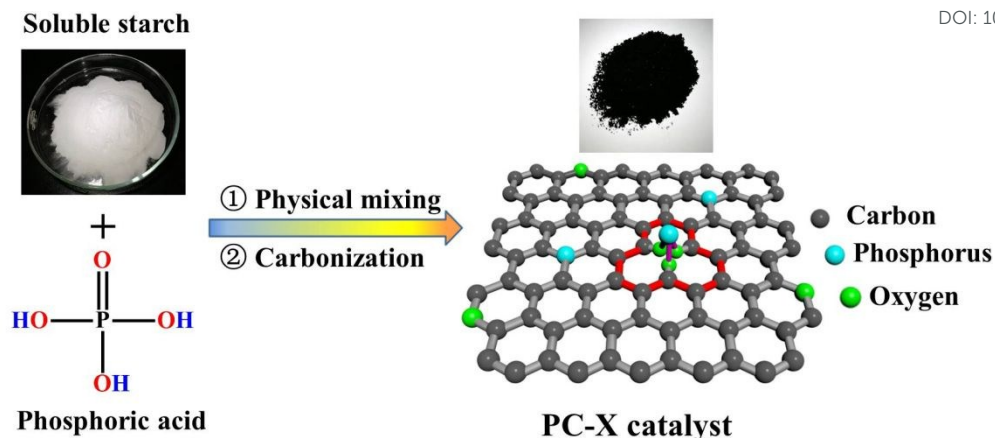
Briefly, soluble starch (5 g) and urea (5 g) were mixed thoroughly in 30 mL of deionized water and dried at 80 °C for 48 h to obtain the N-doped carbon material (NC). The obtained NC was then pyrolyzed at 700 °C to obtain the N-doped catalyst, which was denoted as NC-700. Similarly, the N,P co-doped catalyst was prepared using the same procedures. Soluble starch (5 g), urea (5 g), and phosphoric acid (5.88 g) were used in the preparation, and the mixture was pyrolyzed at 700 °C to obtain the N,P co-doped catalyst (NPC-700).

2.4. Catalytic Aerobic Oxidation of Benzyl Alcohol

Typically, benzyl alcohol (0.5 mmol) and PC-700 (50 mg) were added into a 10 mL thick-walled pressure glass tube that contained 2 mL of deionized water, and then oxygen was continuously bubbled into the solution for 5 min. The tube was then sealed with a Teflon cap, and the solution was stirred at 120 °C. After reaction, the solution samples were sucked out through a syringe, and the solid catalyst was filtered using a 0.2 µm filter. The filtered solution was extracted with ethyl acetate and analyzed using gas chromatography-mass spectrometry (GC-MS, Agilent 5977E).

2.5. Catalyst Characterization

The morphologies of PC-X materials were studied using a transmission electron microscope (TEM, Tecnai G2 F30) and a scanning electron microscope (SEM, HITACHI S-4800). X-ray diffraction (XRD) patterns were recorded on a Rigaku D/max-2400 diffractometer in the range of $2\theta=10-90^\circ$ with Cu- $k\alpha$ radiation. Raman spectra were recorded on a Raman spectrometer (Jobin Yvon Lab Ram HR evolution). An X-ray photoelectron spectrometer (XPS, PHI-5702) was used to investigate the bonding information of PC-X materials. The Brunauer-Emmett-Teller (BET) specific surface areas were measured using nitrogen adsorption-desorption isotherms at 77 K after degassing the samples using a Micromeritics Model ASAP2010 instrument. The pore size distributions were determined using the non-local density functional theory (NLDFT) method with a slit pore model. Fourier transform infrared (FT-IR) spectroscopy was performed on a Bruker spectrometer (VERTEX 70). Thermogravimetric analysis (TGA) was carried out using a TA-Q50 instrument, and PC was heated from 35 to 900 °C under a N₂ atmosphere at a heating rate of 10 °C min⁻¹. Electron paramagnetic resonance (EPR) spectroscopy was recorded on a Bruker A300-9.5/12 instrument.



Scheme 1. The preparation procedures of PC-X catalysts.

3. Results and Discussion

3.1. Preparation process and structural information of PC-X catalysts

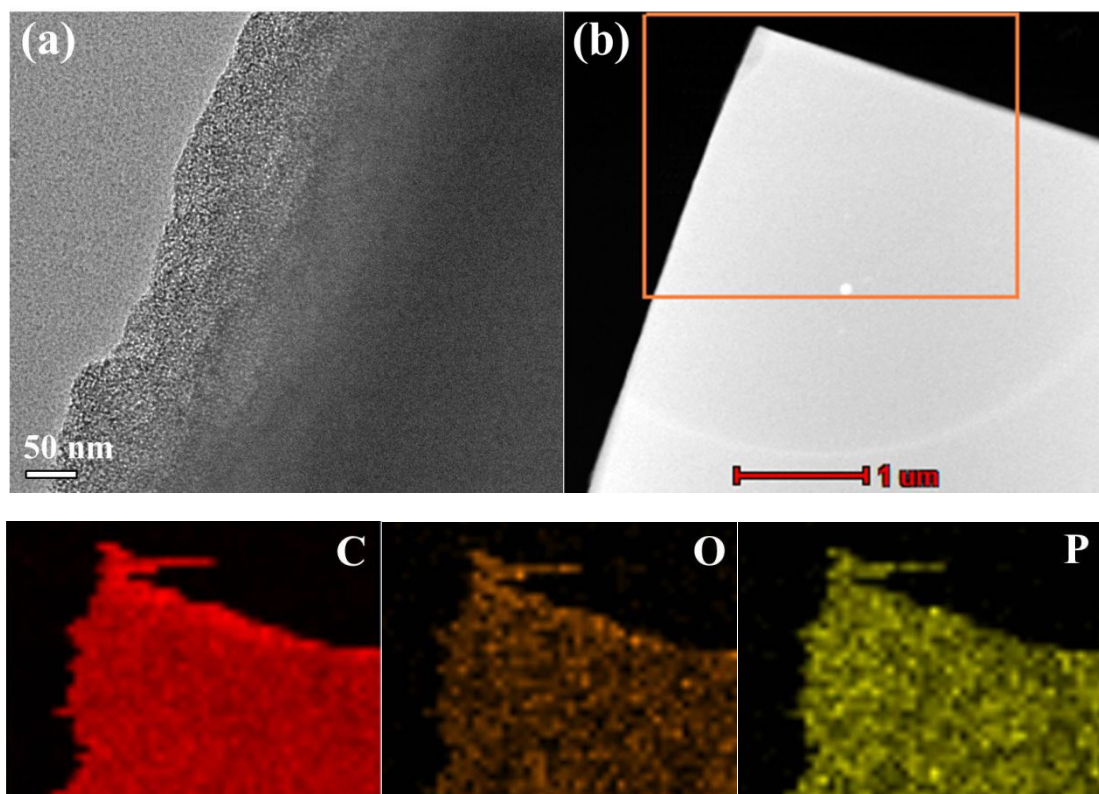


Fig. 1. (a) TEM image of PC-700 catalyst. (b) EDX mapping images of PC-700 for C, O and P elements.

PC-X materials were synthesized using a simple and convenient two-steps process of physical mixing and carbonization (**Scheme 1**). As seen in **Fig. 1a**, the as-fabricated PC-700 catalyst has an overlapping multilayered morphology and a porous structure. Similarly, the

highly wrinkled sheet structure of PC-700 is clear in its SEM image, and this may be attributed to the geometrical deformation that results from the doping of P atoms in the carbon lattice (**Fig. S1c**).³⁸ Other catalysts that are synthesized at different carbonization temperatures (500, 600 and 800 °C) have similar multilayered sheet structures, as seen in their SEM images (**Fig. S1a, b and d**). In addition, the EDX mapping images of the PC-700 catalyst indicate that C, O, and P atoms are evenly distributed on the nanosheets (**Fig. 1b**).

The nitrogen adsorption-desorption isotherm of PC-700 exhibits a type I isotherm, and this indicates the presence of a microporous structure (**Fig. 2a**).⁴² Moreover, the pore size distribution curve of PC-700 shows the presence of micropore centered at 0.64 nm and small mesopore centered at 2.03 nm (**Fig. 2b**). In addition, the calculated BET surface area and pore volume of the PC-700 catalyst are 1612.9 m² g⁻¹ and 0.79 cm³ g⁻¹, respectively (**Table S1, entry 3**). For comparison, the texture parameters of other PC-X catalysts (PC-500, PC-600, and PC-800) are also listed in **Table S1**. Furthermore, the TGA curve indicates three main steps, which were located at 154.7, 558.0 and 786.3 °C with weight losses of 1.8%, 28.9%, and 57.5%, respectively (**Fig. S2**).

3.2. The comparison of reactivity among PC-X and other related catalysts

The prepared PC-X catalysts were applied in the oxidation of benzyl alcohol, and their activity was evaluated using TOF values. With an increase in carbonization temperature, the catalytic activity of the PC-X catalysts first increased and then decreased. PC-700 showed the best catalytic performance with extremely high conversion, selectivity, and TOF value (**Table 1, entries 1 to 4**). As seen in **Table 1, entries 5 and 6**, lower amounts of catalyst and/or reaction temperature both lead to a decrease in conversion. In addition, the poor catalytic performances of the C-700 and PC catalysts indicate that both P doping and high-temperature carbonization are crucial for the high reactivity of the catalysts (**Table 1, entries 7 and 8**). The conversion of the N-doped carbon catalyst (NC-700) was much lower than that of PC-700 (**Table 1, entry 9**). Furthermore, the significant difference in activity between PC-700 and NPC-700 indicates that the intervention of N atoms in the PC-700 catalyst will reduce its reactivity (**Table 1, entries 3 and 10**). Phosphoric acid, which contains only P=O and P-OH bonds was also tested, and it showed no obvious activity in the reaction. This indicates that P=O and P-OH bonds alone cannot act as active species (**Table 1, entry 11**). In addition, the reaction will not happen in the

absence of a catalyst (Table 1, entry 12).

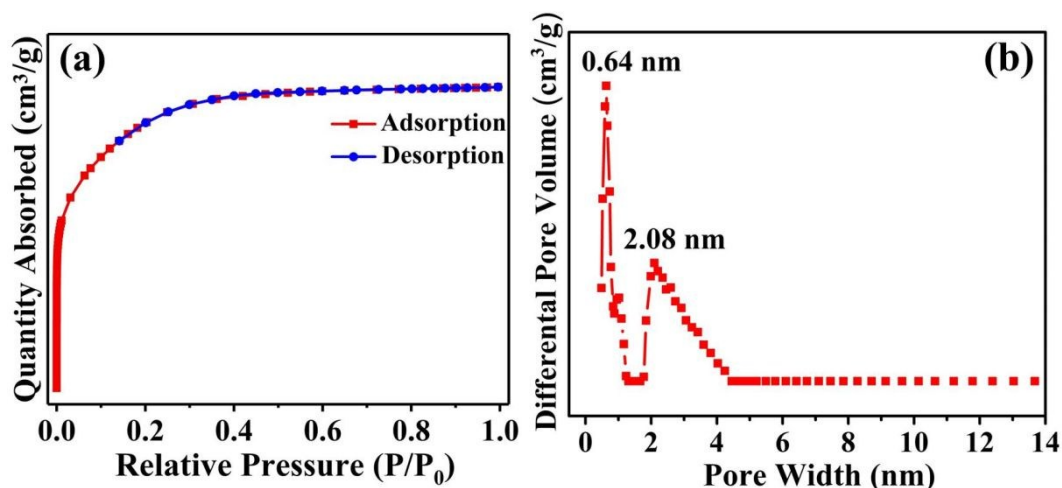
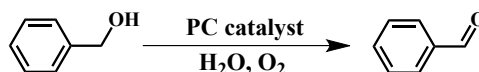


Fig. 2. Nitrogen adsorption-desorption isotherm (a) and pore size distribution curve (b) of PC-700 catalyst.

Table 1. The optimization of reaction conditions for oxidation of benzyl alcohol.^a



Entry	Catalyst/mg	Temp. (°C)	Conv./Sel. (%)	TOF (mol·g ⁻¹ h ⁻¹) ^b
1	PC-500/50	120	59.8/>99	2.49×10 ⁻⁴
2	PC-600/50	120	73.4/>99	3.06×10 ⁻⁴
3	PC-700/50	120	99.9/>99	4.16×10 ⁻⁴
4	PC-800/50	120	96.2/>99	4.01×10 ⁻⁴
5	PC-700/40	120	65.8/>99	3.43×10 ⁻⁴
6	PC-700/50	100	79.8/>99	3.33×10 ⁻⁴
7	PC/50	120	12.9/>99	5.38×10 ⁻⁵
8	C-700/50	120	10.1/>99	4.21×10 ⁻⁵
9	NC-700/50	120	5.3/>99	2.21×10 ⁻⁵
10	NPC-700/50	120	31.2/>99	1.30×10 ⁻⁴
11	H ₃ PO ₄	120	5.7/>99	2.38×10 ⁻⁵
12	none	120	-	-

^a Reaction conditions: 0.5 mmol benzyl alcohol, 50 mg catalyst, 2 mL H₂O, 1 atm O₂, 24 h. The conversion and selectivity were determined by GC-MS.

^b Turnover frequency (TOF) = $\frac{\text{mole of converted substrate}}{\text{g catalyst} \times \text{reaction time (h)}}$.

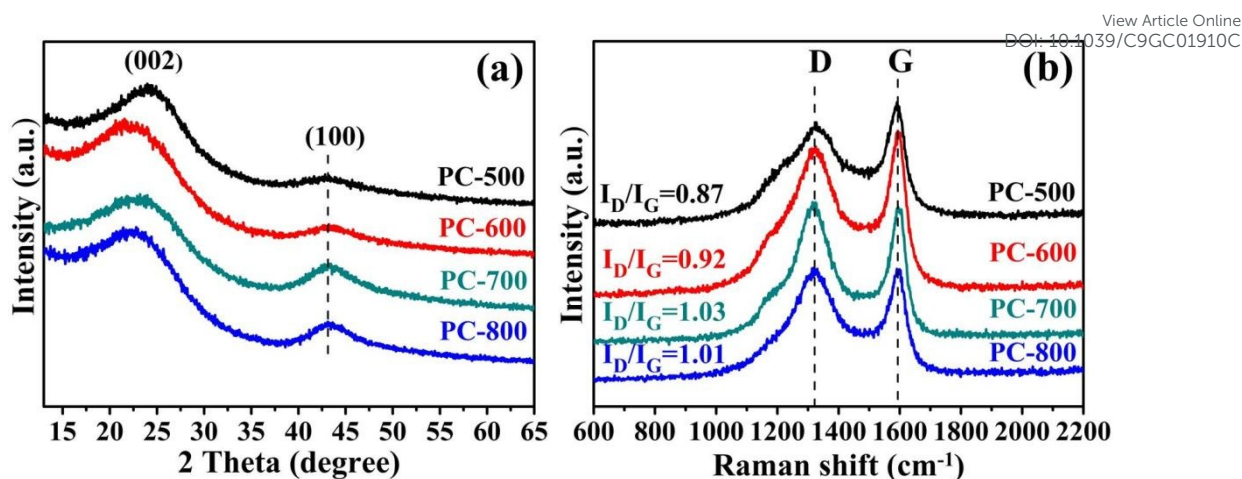


Fig. 3. XRD patterns (a) and Raman spectra (b) of PC-500, PC-600, PC-700 and PC-800 catalysts.

3.3. Investigation of the cause of defects formation and the intrinsic active sites in PC-X catalysts

A series of characterizations, such as Raman spectroscopy, XPS, and FT-IR were performed to explore the possible active sites of PC-X catalysts. The XRD patterns (**Fig. 3a**) indicate that the PC-X catalysts are carbon materials and show two main peaks at around 24° and 43° , which represent the (002) and (100) planes of graphitic carbon, respectively.⁴³ As seen in **Fig. 3b**, the D and G bands, which are located at 1325 cm^{-1} and 1595 cm^{-1} , respectively, represent lattice defects and the graphitic phase in catalysts, respectively.^{44, 45} It is determined that the relative intensity of the two bands (I_D/I_G) in the PC-700 catalyst is the highest, and this indicates the highest density of defects in its framework. On the contrary, the PC-500 catalyst has the lowest density of defects.

XPS spectra were recorded to obtain crucial information regarding the P-doping content, the detailed bonding configuration of P atoms, and the possible cause of the formation of defects. As seen in the wide scan spectra (**Fig. S3**), all of the PC-X catalysts contain C, O, and P, which is also confirmed by the EDX spectrum (**Fig. S4**). The XPS high-resolution C1s spectra consist of four peaks located at 284.6 eV, 285.2 eV, 285.9 eV and 289.3 eV corresponding to $\text{SP}^2\text{ C}$, $\text{SP}^3\text{ C}$, C-P and O-C=O species, respectively (**Fig. S5**). The detailed P-doping concentrations that were determined from the wide scan spectra of different PC-X catalysts are listed in **Table 2**. It is worth noting that a well linear correlation was found between the P-doping concentration

and the values of I_D/I_G (**Fig. S6a**), and also between the P-O species concentration and the values of I_D/I_G (**Fig. S6b**), which indicates that the formation of defects in the PC-X catalysts is closely related to P-O species doping. Moreover, the TOF values in the oxidation reaction are linearly correlated with the values of I_D/I_G in different PC-X catalysts (**Fig. S6c**). However, there is no obvious correlation with the surface area of the PC-X catalysts (**Table S1, entries 1 to 4**). Thus, it can be concluded that the catalytic activity of the PC-X catalysts is significantly associated with the formation of defects.

To study the relationship between different P-containing groups and catalytic activity, XPS high-resolution P2p and O1s spectra were recorded and analyzed. As seen in **Fig. 4a**, the spectra were mainly composed of two peaks at 132.5 ± 0.1 and 134.0 ± 0.1 eV, which correspond to P-C and P-O type of species. In addition, the O1s spectra has three main peaks at 531.0 ± 0.1 eV, 532.4 ± 0.2 eV, and 533.6 ± 0.2 eV, which correspond to C/P=O, C/P-O-C, and C/P-OH (**Fig. 4b**). The calculated P-C and P-O contents based on total P content and high-resolution P2p spectra are listed in **Table 2, entries 1 to 4**. Moreover, as shown in **Fig. S6d**, the TOF values in the oxidation reaction changes linearly with the calculated P-O species concentrations, while there is no obvious correlation with the P-C contents. This indicates that P-O species are closely associated with the catalytic activity of PC-X catalysts in oxidation reaction. Moreover, the calculated contents of different species in the O1s spectra indicate that the content of C/P-OH species in the PC-700 catalyst is lower than that of other PC-X catalysts, whereas the contents of C/P=O and C/P-O-C species in the PC-700 catalyst are similar to or even higher than those of other PC-X catalysts (**Table S2, entries 1 to 4**); besides, the PC-700 catalyst shows the highest catalytic activity, which further confirms the conclusion mentioned above. Furthermore, in the FT-IR spectra, the intensity of the peaks at 1035 cm^{-1} (C-O-P) for the PC-700 and PC-800 catalysts are much higher than those for the PC-500 and PC-600 catalysts (**Fig. S7**); besides, both PC-700 and PC-800 showed excellent and similar catalytic activity.³⁸ In conclusion, from all the results obtained above, it can be concluded that P-O-C species and the defects caused by P-O species doping may be the crucial active sites for aerobic oxidation reaction.

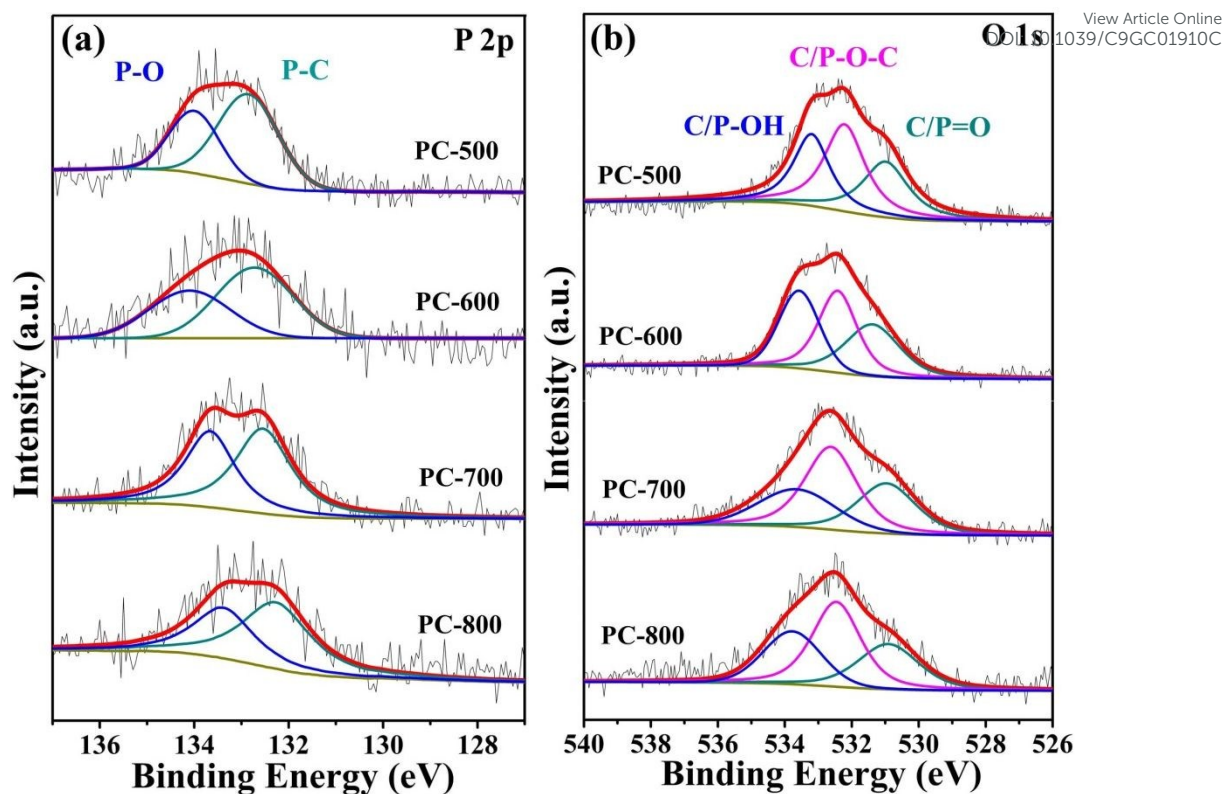


Fig. 4. XPS high-resolution P 2p (a) and O 1s (b) spectra of PC-X catalysts, i.e., PC-500, PC-600, PC-700 and PC-800, respectively.

Table 2. XPS total and calculated element contents in different PC-X catalysts.

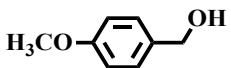
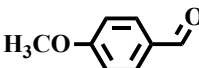
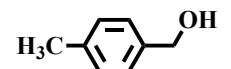
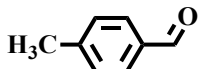
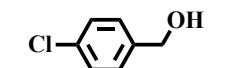


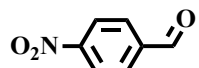
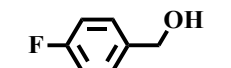
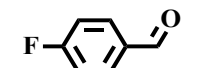
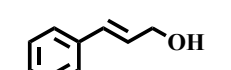
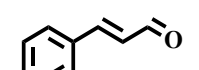

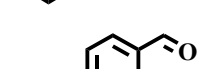
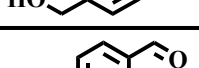
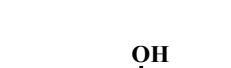
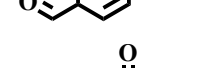
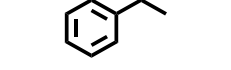
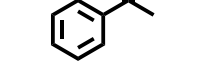
Entr y	Catalyst	Total %			Calculated %	
		C [at. %]	P [at. %]	O [at. %]	P-C [at. %]	P-O [at. %]
1	PC-500	92.05	0.41	7.54	0.26	0.15
2	PC-600	92.51	0.61	6.88	0.36	0.25
3	PC-700	93.19	0.96	5.85	0.53	0.43
4	PC-800	95.58	0.90	3.52	0.54	0.36

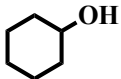
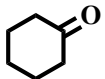


3.4. Substrate scope test of PC-700 catalyst in selective aerobic oxidation of various alcohols

The reaction activity of the PC-700 catalyst was further investigated using different types of substrates, including aromatic, alicyclic, heterocyclic, and aliphatic alcohols. For aromatic alcohols, the alcohols that have electron-donating groups ($-\text{OCH}_3$, $-\text{CH}_3$) are more effectively converted into the corresponding products than the alcohols that have election-withdrawing

groups (-Cl, -NO₂) (**Table 3, entries 1 to 4**). This is quite different from the situation of the reaction catalyzed by N-doped carbon materials, which there are no obvious differences between the substrates with electron-withdrawing groups or those with electron-donating groups.³⁹ The aromatic alcohol with a fluoro-group is a special case, it was catalyzed effectively as an aromatic alcohol with an electron-donating group (**Table 3, entry 5**). This may be attributed to the very small atomic size of fluorine. Cinnamyl alcohol as a kind of unsaturated aromatic alcohol was also catalyzed with high conversion (>99%) and excellent selectivity (>98%) (**Table 3, entry 6**). The aromatic alcohol that has two hydroxy groups was oxidized to two products (95.3% conversion), of which 4-hydroxybenzaldehyde is the main product (**Table 3, entry 7**). Secondary aromatic alcohols showed higher reactivity than alicyclic alcohol and heterocyclic alcohol (**Table 3, entries 8 to 10**). In addition, aliphatic alcohols cannot be catalyzed in this reaction (**Table 3, entry 11**).

Table 3. The selective aerobic oxidation of different alcohols on PC-700 under the optimal condition. ^a

Entry	Substrate	Product	Time (h)	Conv./ Sel.(%)	TOF ^b (mol·g ⁻¹ h ⁻¹)
1			22	99.6/>99	4.53×10 ⁻⁴
2			24	99.8/>99	4.16×10 ⁻⁴
3			24	73.1/98.3	2.99×10 ⁻⁴
4			24	16.6/>99	6.92×10 ⁻⁵
5			24	97.8/>99	4.08×10 ⁻⁴
6			24	99.3/98.7	4.10×10 ⁻⁴
7		 	24	80.9/>99 14.4/>99	3.37×10 ⁻⁴ 6.00×10 ⁻⁵
8			24	27.3/>99	1.14×10 ⁻⁴
9			24	5.8/>99	2.42×10 ⁻⁵

10			24	2.1/>99	8.75×10 ⁻⁶
11			24	<1/>99	-

View Article Online
DOI: 10.1039/C9GC01910C

^a Reaction conditions: 0.5 mmol substrate, 50 mg PC-700, 2 mL H₂O, 1 atm O₂, 120 °C. The conversion and selectivity were determined by GC-MS.

$$^b \text{Turnover frequency (TOF)} = \frac{\text{mole of converted substrate}}{\text{g catalyst} \times \text{reaction time (h)}}$$

3.5. Control experiments and kinetic research of aerobic oxidation of benzyl alcohol

To further investigate the aerobic oxidation of benzyl alcohol catalyzed by the PC-700 catalyst, a series of control experiments have been specifically designed. First, to determine the role that oxygen plays in the reaction, control experiments were performed in different gaseous atmospheres. As listed in **Table 4**, benzyl alcohol could be completely converted into corresponding product in 24 h with the existence of oxygen (**Table 4, entry 1**). To further illustrate the good chemoselectivity in this reaction, the control experiment was carried out with a longer reaction time (48 h) in the same reaction conditions, there are no obvious differences in selectivity compared with that of original reaction (**Table 4, entry 2**). However, when reaction was performed in an atmosphere of air, a relatively lower conversion (24.4 %) was obtained than the case that oxygen was the reaction gas (**Table 4, entry 3**). In addition, a poor conversion was occurred when the reaction was performed in an inert atmosphere (N₂) for even 48 h (**Table 4, entries 4 and 5**). Notably, when the reaction was performed in an inert atmosphere for 24 h, there was poor reactivity with a very low conversion (3.60%), while when oxygen was introduced into the reaction system and reacted for another 24 h, the conversion recovered back to 61.3% (**Table 4, entry 6**). Thus, it is clear that the participation of O₂ is crucial in the catalytic process.

Table 4. Catalytic activity test on PC-700 catalyst using different oxidants.^a

Entry	Catalyst	Oxidant	Time (h)	Conv./Sel. (%)	TOF ^b (mol·g ⁻¹ ·h ⁻¹)
1	PC-700	O ₂	24	99.9/>99	4.16×10 ⁻⁴
2	PC-700	O ₂	48	99.9/>99	2.08×10 ⁻⁴
3	PC-700	Air	24	24.4/>99	1.02×10 ⁻⁴
4	PC-700	N ₂	24	3.60/>99	1.50×10 ⁻⁵
5	PC-700	N ₂	48	3.86/>99	8.04×10 ⁻⁶

6	PC-700	N ₂ to O ₂	24 to 48	61.3/>99	1.28×10 ⁻⁴
---	--------	----------------------------------	----------	----------	-----------------------

^a Reaction conditions: 0.5 mmol benzyl alcohol, 50 mg PC-700, 2 mL H₂O, 120 °C. The conversion and selectivity were determined by GC-MS.

$$^b \text{Turnover frequency (TOF)} = \frac{\text{mole of converted substrate}}{\text{g catalyst} \times \text{reaction time (h)}}$$

To study the reactivity of PC-X catalysts in the aerobic oxidation of benzyl alcohol, the kinetic research is crucially important. Thus, the reaction was performed at a series of reaction temperatures (333-393 K). To complete the plot of $\ln k$ versus $1/T$, the rate constants (k) were calculated from the fitting lines shown in **Fig. 5a**. The apparent activation energy (E_a) was calculated to be 25.70 KJ·mol⁻¹ using the Arrhenius equation and the slope and intercept shown in **Fig. 5b** (-3091.11 and -4.76, respectively). Moreover, the PC-700 catalyst was compared with other catalysts reported in previous works to further evaluate its catalytic reactivity in the oxidation of benzyl alcohol. As seen in **Table 5**, the PC-700 catalyst shows higher catalytic activity than mono-heteroatom-doped catalysts and similar catalytic activity to that of dual-heteroatom-doped catalysts with a relatively high TOF value under the same reaction conditions. Furthermore, the E_a value of the reaction (25.70 KJ·mol⁻¹) that is catalyzed by the PC-700 catalyst is lower than that of reported metal-free catalysts and even noble metal catalysts catalyzed aerobic oxidation of benzyl alcohol (**Table 5, entries 1 to 7**). Thus, the PC-700 catalyst exhibits remarkable catalytic performance by lowering the E_a value of the reaction.

Table 5. The comparison of catalytic activity and activation energy of different catalysts in benzyl alcohol oxidation.

Entry	Catalyst/mg	Oxidant	Substrate (mmol)	Temp. (°C)	TOF (mol·g ⁻¹ h ⁻¹)	E _a (KJ·mol ⁻¹)	Ref.
1	nitrogen-doped Graphene/30	1 atm O ₂	0.1	80	4.83×10 ⁻⁵	56.1	39
2	modified GO/50	2 atm O ₂	0.25	100	1.55×10 ⁻⁴	-	46
3	P-doped porous Carbon/3	1 atm O ₂	0.0185	100	2.10×10 ⁻⁴	49.6	38
4	P and S dual-doped graphitic porous carbon/100	1 atm O ₂	1.0	100	3.75×10 ⁻⁴	32.0	40

5 ^a	5 wt% Ru/C	1 atm air	1.1	120	29/h ⁻¹	32.0	View Article Online DOI: 10.1039/C9GC01910C
6 ^b	2.5 mol% Ru/Al ₂ O ₃	1 atm O ₂	1.0	83	0.4/h ⁻¹	51.4	41
7	P-doped porous Carbon/50	1 atm O ₂	0.5	80	2.59×10 ⁻⁴	25.7	This Work
				100	3.33×10 ⁻⁴		

$${}^{a,b} \text{Turnover frequency (TOF)} = \frac{\text{mole of converted substrate}}{\text{mole of metal} \times \text{reaction time (h)}}$$

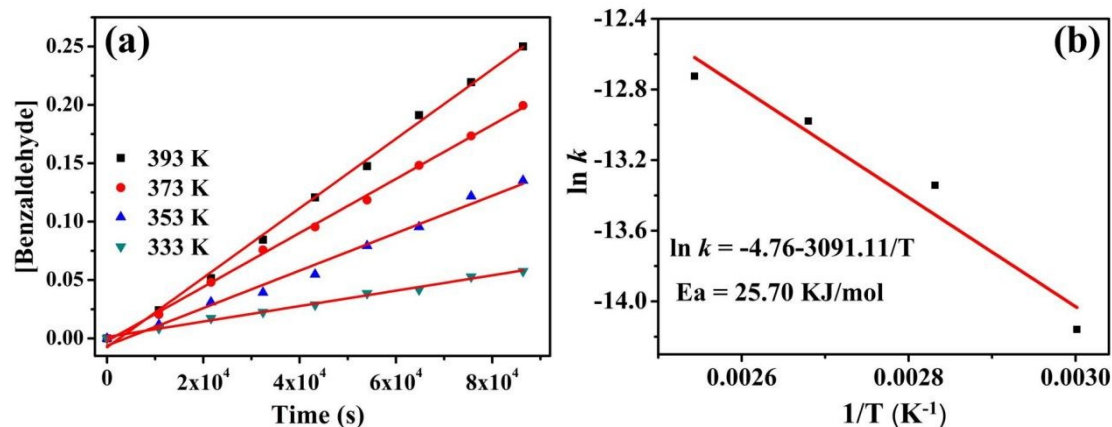


Fig. 5. (a) Plots of concentration of benzaldehyde versus reaction time for the oxidation of benzyl alcohol catalyzed by PC-700 catalyst at different reaction temperatures. Reaction conditions: 0.5 mmol benzyl alcohol, 50 mg PC-700, 2 mL H₂O, 1 atm O₂. (b) Arrhenius plot for the benzyl alcohol oxidation.

To determine if free radical intermediates were generated in the aerobic oxidation of benzyl alcohol catalyzed by the PC-700 catalyst, a control experiment was carried out in the presence of a radical inhibitor (BHT). As listed in **Table 6**, the conversion and selectivity were hardly affected by the addition of BHT, suggesting no radical intermediates were generated in the reaction. The same conclusion was also confirmed by EPR characterization using 5,5-dimethyl-1-pyrroline N-oxide (DMPO) as the spin trap, which shows no obvious signal in the spectrum (**Fig. S8**). This result is different from the reactions catalyzed by GO and N-doped metal-free catalysts; such reactions are closely related to the free radical intermediates formed in the catalytic process.^{39, 48}

Table 6. The control experiment of benzyl alcohol oxidation in the presence of a radical inhibitor.^a

Entry	Catalyst	Radical inhibitor	Conv./Sel. (%)
1	PC-700	none	99.9/>99
2 ^b	PC-700	BHT	98.2/>99

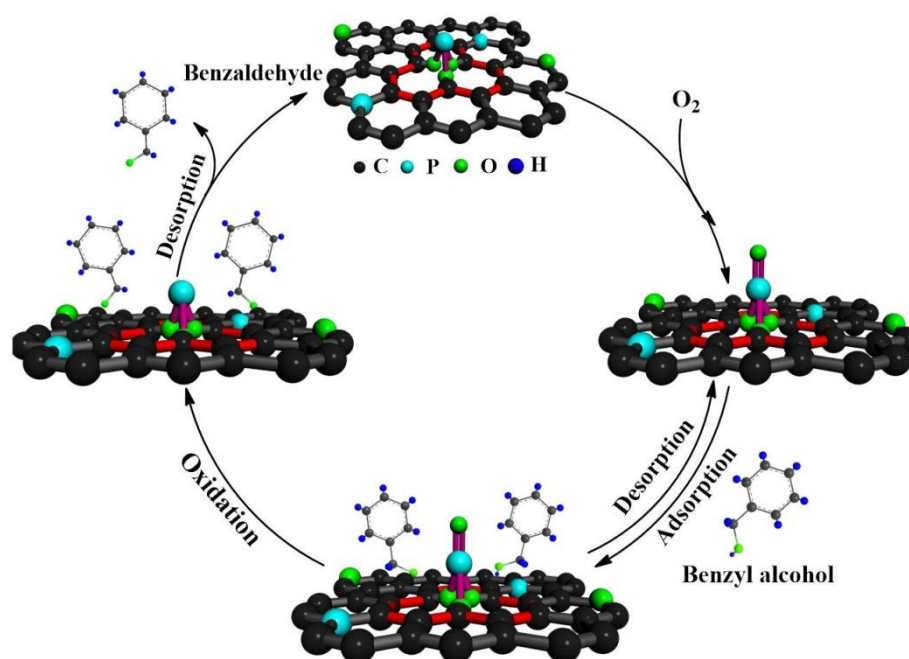
^a Reaction conditions: 0.5 mmol benzyl alcohol, 50 mg PC-700, 2 mL H₂O, 1 atm O₂, 120 °C, 24 h. The conversion and selectivity were determined by GC-MS. ^b 0.25 mmol butylated hydroxytoluene (BHT) was dissolved in 200 μL ethanol and then added in the reaction solution.

3.6. The detailed analysis of active sites and catalytic mechanism

On the basis of the characterizations and control experiments, important information concerning active sites and the catalytic mechanism was collected as follows: (1) The intervention of N inhibits the reactivity of PC-X catalysts. (2) The formation of defects in PC-X catalysts is attributed to the doping of P-O species. (3) The P-O-C species and defects caused by P-O species doping are the active sites for aerobic oxidation reactions. (4) It is clear that the participation of O₂ is crucial in the aerobic oxidation of benzyl alcohol when the reaction is catalyzed by PC-X catalysts. (5) The PC-700 catalyst exhibits a lower E_a value of aerobic oxidation than other reported metal-free and even noble metal catalysts, and thus it has remarkable catalytic capability. (6) There are no radical intermediates generated in the aerobic oxidation reaction, which is quite different from when the same reaction that was catalyzed by other heteroatom-doped catalysts.

On the basis of all of above the factors, a reasonable mechanism was proposed and shown in **Scheme 2**. The control experiment in the absence of oxygen showed poor activity, suggesting the P-containing active species in PC-700 catalyst are not qualified with enough oxidation ability; besides, oxygen is needed to participate in the reaction process. Accordingly, in the first step, oxygen should be adsorbed on the nearby active sites of PC-X catalysts to form active oxygen species. From the control experiment in the presence of BHT and EPR characterization, it is clear that no free radical intermediates were generated in the catalytic process. Therefore, a new P-containing active intermediate with a higher valence state (O-P=O) was more likely generated with the assistance of oxygen in the first step. After the first step, oxygen was reduced into hydrogen peroxide in aqueous solution. More importantly, the generated hydrogen peroxide would immediately decompose into oxygen and water at high reaction temperature,

and the generated oxygen will be back into the reaction system. That is the reason why the oxidation process can be finished with limited oxygen. In addition, from the linear relationships between P-O species concentrations, I_D/I_G values, and TOF values, it is reasonable to assume that the active sites were probably located around the defects on the PC-X catalysts. Therefore, in the second step, the benzyl alcohol was adsorbed and then oxidized by new P-containing active intermediates locally around the defects. After the oxidation of benzyl alcohol, the new P-containing active intermediates were reduced to the original active species. At last, the catalytic cycle finished with the desorption of products.



Scheme 2. A possible reaction mechanism for the aerobic oxidation of benzyl alcohol catalyzed by PC-700 catalyst with the existence of oxygen.

3.7. The evaluation of recyclability and stability of PC-700 catalyst

The recyclability and stability of the PC-700 catalyst were evaluated using a recycling test of aerobic oxidation of benzyl alcohol and several related characterizations of the reused catalyst. As clearly seen in **Fig. 6**, the PC-700 catalyst shows outstanding stability in the recycling test with relatively high conversion (89.8%) and excellent selectivity (>99%) even after 8 cycles. In addition, the remarkable structural stability of PC-700 was confirmed by a TEM image of the reused PC-700 catalyst, which shows the unchanged overlapping multilayered morphology (**Fig. S9**). A PXRD pattern of the reused PC-700 catalyst also shows

that it is unchanged (**Fig. S10a**), and the value of I_D/I_G that is calculated from the Raman spectrum of the reused catalyst is very close to that of the fresh catalyst (**Fig. S10b**). This indicates the stability of the physical structure of the PC-700 catalyst. Moreover, as seen in the XPS spectra of the PC-700 catalyst that was recycled 8 times, the contents of C, O, and P are similar to those of fresh the catalyst (**Fig. S11**); Besides, there are no obvious differences between the P2p and O1s spectra of the fresh and reused PC-700 catalyst (**Fig. S12 a and b**). Furthermore, as listed in **Table S3 and 4**, the contents of P-containing species in the reused PC-700 catalyst that were calculated based on the high-resolution P2p and O1s spectra are also almost unchanged. These results have well demonstrated that the PC-700 catalyst has extraordinary performances both in recyclability and stability.

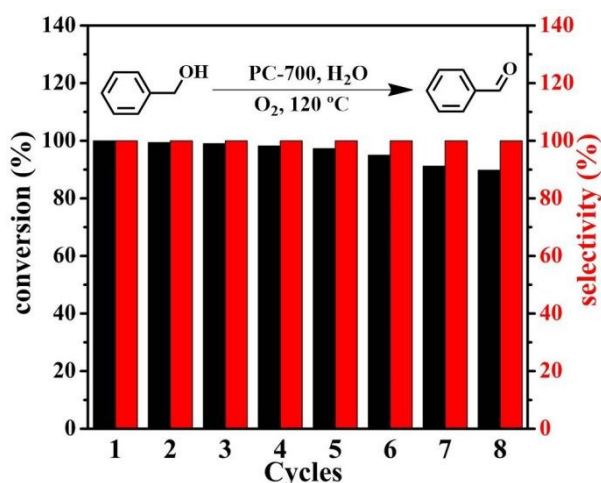


Fig. 6. Recycling test of PC-700 catalyst in benzyl alcohol oxidation. Reaction conditions: 0.5 mmol benzyl alcohol, 50 mg PC-700, 2 mL H₂O, 1 atm O₂, 120 °C, 24 h.

4. Conclusions

In summary, PC-X materials were prepared via a scalable two-steps approach using cost-efficient and easily available soluble starch and phosphoric acid, which makes the as-prepared catalysts cost-efficient and environment-friendly. The as-fabricated PC-700 proved to be an efficient metal-free catalyst in the aerobic oxidation of benzyl alcohol, achieving full conversion (>99%) and remarkable selectivity (>99%). On the basis of the related characterizations and experimental results, the P-O-C species and the defects caused by P-O species doping were demonstrated to be the active sites for the oxidation reaction. The PC-700 catalyst showed better catalytic performance than mono-heteroatom-doped catalysts and

comparable catalytic performance to dual-heteroatom-doped catalysts. It is expected that this work provides an extremely simple and scalable way to fabricate HDCMs that have great potential in metal-free catalysis.

View Article Online
DOI: 10.1039/C9GC01910C

Conflicts of interest

There are no conflicts to declare.

Supporting Information

Supporting Information is available from the publication website.

Acknowledgements

This work was supported by the Natural Science Foundation of Gansu (No. 18JR3RA274).

References

1. T. Mallat and A. Baiker, *Chem. Rev.*, 2004, **104**, 3037-3058.
2. A. Abad, P. Concepción, A. Corma and H. García, *Angew. Chem. Int. Ed.*, 2005, **44**, 4066-4069.
3. D. I. Enache, J. K. Edwards, P. Landon, B. Solsona-Espriu, A. F. Carley, A. A. Herzing, M. Watanabe, C. J. Kiely, D. W. Knight and G. J. Hutchings, *Science*, 2006, **311**, 362-365.
4. C. Aellig, C. Girard and I. Hermans, *Angew. Chem. Int. Ed.*, 2011, **50**, 12355-12360.
5. A. Tanaka, K. Hashimoto and H. Kominami, *J. Am. Chem. Soc.*, 2012, **134**, 14526-14533.
6. Y. Kuang, N. M. Islam, Y. Nabaie, T. Hayakawa and M.-a. Kakimoto, *Angew. Chem. Int. Ed.*, 2010, **49**, 436-440.
7. A. Dijkstra, A. Marino-González, A. Mairata i Payeras, I. W. C. E. Arends and R. A. Sheldon, *J. Am. Chem. Soc.*, 2001, **123**, 6826-6833.
8. M. Conte, H. Miyamura, S. Kobayashi and V. Chechik, *J. Am. Chem. Soc.*, 2009, **131**, 7189-7196.
9. C. Parmeggiani, C. Matassini and F. Cardona, *Green Chem.*, 2017, **19**, 2030-2050.
10. C. Parmeggiani and F. Cardona, *Green Chem.*, 2012, **14**, 547-564.
11. M. Antonietti and M. Oschatz, *Adv. Mater.*, 2018, **30**, 1706836.
12. M. Antonietti, N. Lopez-Salas and A. Primo, *Adv. Mater.*, 2018, **31**, 1805719.
13. H. Fei, J. Dong, C. Wan, Z. Zhao, X. Xu, Z. Lin, Y. Wang, H. Liu, K. Zang, J. Luo, S. Zhao, W. Hu, W. Yan, I. Shakir, Y. Huang and X. Duan, *Adv. Mater.*, 2018, **30**, 1802146.
14. M. Khan, M. N. Tahir, S. F. Adil, H. U. Khan, M. R. H. Siddiqui, A. A. Al-warthan

- and W. Tremel, *J. Mater. Chem. A*, 2015, **3**, 18753-18808.
15. I. Ocsoy, B. Gulbakan, T. Chen, G. Zhu, Z. Chen, M. M. Sari, L. Peng, X. Xiong, X. Fang and W. Tan, *Adv. Mater.*, 2013, **25**, 2319-2325.
 16. R. H. Baughman, A. A. Zakhidov and W. A. de Heer, *Science*, 2002, **297**, 787-792.
 17. X. Liu and L. Dai, *Nat. Rev. Mater.*, 2016, **1**, 16064.
 18. X. Wang, G. Sun, P. Routh, D.-H. Kim, W. Huang and P. Chen, *Chem. Soc. Rev.*, 2014, **43**, 7067-7098.
 19. K. N. Wood, R. O'Hayre and S. Pylypenko, *Energy Environ. Sci.*, 2014, **7**, 1212-1249.
 20. Z. H. Li, M. F. Shao, Q. H. Yang, Y. Tang, M. Wei, D. G. Evans and X. Duan, *Nano Energy*, 2017, **37**, 98-107.
 21. Y. Zhao, L. J. Yang, S. Chen, X. Z. Wang, Y. W. Ma, Q. Wu, Y. F. Jiang, W. J. Qian and Z. Hu, *J. Am. Chem. Soc.*, 2013, **135**, 1201-1204.
 22. D. Yu, Y. Xue and L. Dai, *J. Phys. Chem. Lett.*, 2012, **3**, 2863-2870.
 23. W. Lei, Y.-P. Deng, G. Li, Z. P. Cano, X. Wang, D. Luo, Y. Liu, D. Wang and Z. Chen, *ACS Catal.*, 2018, **8**, 2464-2472.
 24. D.-S. Yang, D. Bhattacharjya, S. Inamdar, J. Park and J.-S. Yu, *J. Am. Chem. Soc.*, 2012, **134**, 16127-16130.
 25. Z.-W. Liu, F. Peng, H.-J. Wang, H. Yu, W.-X. Zheng and J. Yang, *Angew. Chem. Int. Ed.*, 2011, **50**, 3257-3261.
 26. X. Zhang, Z. Lu, Z. Fu, Y. Tang, D. Ma and Z. Yang, *J. Power Sources*, 2015, **276**, 222-229.
 27. J. Yi, Y. Qing, C. Wu, Y. Zeng, Y. Wu, X. Lu and Y. Tong, *J. Power Sources*, 2017, **351**, 130-137.
 28. S. K. Ramasahayam, Z. Hicks and T. Viswanathan, *ACS Sustain. Chem. Eng.*, 2015, **3**, 2194-2202.
 29. R. Gao, L. Pan, J. Lu, J. Xu, X. Zhang, L. Wang and J.-J. Zou, *ChemCatChem*, 2017, **9**, 4287-4294.
 30. M. Borghei, J. Lehtonen, L. Liu and O. J. Rojas, *Adv. Mater.*, 2018, **30**, 1703691.
 31. M. Danish and T. Ahmad, *Renew. Sust. Energ. Rev.*, 2018, **87**, 1-21.
 32. O. Fromm, A. Heckmann, U. C. Rodehorst, J. Frerichs, D. Becker, M. Winter and T. Placke, *Carbon*, 2018, **128**, 147-163.
 33. S. Y. Gao, X. G. Li, L. Y. Li and X. J. Wei, *Nano Energy*, 2017, **33**, 334-342.
 34. J. Niu, R. Shao, J. J. Liang, M. L. Dou, Z. L. Li, Y. Q. Huang and F. Wang, *Nano Energy*, 2017, **36**, 322-330.
 35. Y. Gong, D. Li, C. Luo, Q. Fu and C. Pan, *Green Chem.*, 2017, **19**, 4132-4140.
 36. J. Han, S. Y. Jeong, J. H. Lee, J. W. Choi, J. W. Lee and K. C. Roh, *ACS Sustain. Chem. Eng.*, 2019, **7**, 2471-2482.
 37. G.-J. t. Brink, I. W. C. E. Arends and R. A. Sheldon, *Science*, 2000, **287**, 1636-1639.
 38. M. A. Patel, F. Luo, M. R. Khoshi, E. Rabie, Q. Zhang, C. R. Flach, R. Mendelsohn, E. Garfunkel, M. Szostak and H. He, *Acs Nano*, 2016, **10**, 2305-2315.
 39. J. Long, X. Xie, J. Xu, Q. Gu, L. Chen and X. Wang, *ACS Catal.*, 2012, **2**, 622-631.
 40. M. A. Patel, F. Luo, K. Savaram, P. Kucheryavy, Q. Xie, C. Flach, R. Mendelsohn, E. Garfunkel, J. V. Lockard and H. He, *Carbon*, 2017, **114**, 383-392.
 41. K. Yamaguchi and N. Mizuno, *Chem.-Eur. J.*, 2003, **9**, 4353-4361.

42. Z. Qin, K. A. Cychosz, G. Melinte, H. El Siblani, J.-P. Gilson, M. Thommes, C. Fernandez, S. Mintova, O. Ersen and V. Valtchev, *J. Am. Chem. Soc.*, 2017, **139**, 17273-17276. View Article Online
DOI: 10.1039/C9GC01910C
43. M. Fan, J. Wu, J. Yuan, L. Deng, N. Zhong, L. He, J. Cui, Z. Wang, S. K. Behera, C. Zhang, J. Lai, B. I. Jawdat, R. Vajtai, P. Deb, Y. Huang, J. Qian, J. Yang, J. M. Tour, J. Lou, C.-W. Chu, D. Sun and P. M. Ajayan, *Adv. Mater.*, 2019, **31**, 1805778.
44. X. Sun, W. Wang, L. Qiu, W. Guo, Y. Yu and H. Peng, *Angew. Chem. Int. Ed.*, 2012, **51**, 8520-8524.
45. L. Qie, Y. Lin, J. W. Connell, J. Xu and L. Dai, *Angew. Chem. Int. Ed.*, 2017, **56**, 6970-6974.
46. S. Zhu, Y. Cen, M. Yang, J. Guo, C. Chen, J. Wang and W. Fan, *Appl. Catal. B: Environ.*, 2017, **211**, 89-97.
47. H. Watanabe, S. Asano, S.-i. Fujita, H. Yoshida and M. Arai, *ACS Catal.*, 2015, **5**, 2886-2894.
48. D. R. Dreyer, H.-P. Jia and C. W. Bielawski, *Angew. Chem. Int. Ed.*, 2010, **49**, 6813-6816.

Graphic abstract

